2024 IEEE International Conference on Robotics and Automation (ICRA 2024)
May 13-17, 2024. Yokohama, Japan

Ospreys-inspired Self-takeoff Strategy of An Eagle-scale Flapping-wing Robot: System Design and Flight Experiments

Haoyu Wang, Wenfu Xu, Linpo Hou, and Erzhen Pan

Abstract— **In this work, we achieved a self-takeoff of an eagle-scale flapping-wing robot for the first time. Inspired by the takeoff process of Ospreys, we propose a bio-inspired takeoff strategy, then discuss the dynamic model and the requirements for self-takeoff. Based on the requirements of flight strategy, we designed a system with two parts, including a flapping-wing aircraft with a wingspan of 1.8m and a take-off weight of 870g, and an auxiliary platform with an initial pitch angle adjustment function. In order to explore the differences in the take-off process under different conditions, we conduct the flight experiments under different time-averaged thrust-to-weight ratios (0.745-0.876) and launch angles (45°-90°). The results of flight experiments confirmed the theoretical analysis that the flapping-wing robot can achieve self-takeoff with no potential energy cost and maintain high maneuverability (The video shows a rapid climb immediately after takeoff) even when the time-averaged thrust-to-weight ratio is smaller than 1. This is significantly different from conventional rotary-wing and vertical take-off and landing (VTOL) UAVs. This work solves the challenge of self-takeoff for large-scale flapping-wing robots using a designable method and demonstrates the superior performance potential of flapping-wing robots compared to conventional UAVs.**

I. Introduction

Large-scale flapping-wing aircraft have attracted wide attention from scholars in recent years due to their heavier payload, longer endurance, and larger design space of mechanism [1]-[4]. However, in terms of application, most flapping-wing robots cannot self-takeoff but have to rely on catapult devices or be launched by an operator, which greatly limits their application scenarios, such as secondary take-off after perching. The goal of this research is to study the strategy of self-takeoff and develop an eagle-scale flapping-wing aircraft with self-takeoff capability.

For rotary-wing aircraft and VTOL (vertical take-off and landing UAVs), self-takeoff is a mature technology. Many micro-flapping-wing aircraft can also achieve vertical take-off and hover [5]-[7]. However the implementation of these technologies requires strict requirements on the drone's power system and weight, that is, the thrust-to-weight ratio is greater than 1, which results in the drone not being able to carry enough payload, or need to strengthen the power system leads to the increase of weight. For large-scale flapping-wing aircraft, the thrust is generated by wings with large size and inertia, the weight cost is huge or even unacceptable if they meet the requirement of a thrust-to-weight ratio greater than 1.

Some research in the field of biology also indicates the self-takeoff of large-scale flapping-wing drones. Some studies suggest that the thrust provided by the bird legs is the key to the successful takeoff of birds [8]-[10],[14]. This view holds that birds must have sufficient initial velocity provided by structures such as bird legs during takeoff. This may be a feasible scheme, but as the landing gear of fixed-wing aircraft, the bird-leg mechanism increases the extra weight, the aerodynamic resistance, and reduces the reliability of the system.

Combining the above considerations, we hope to find a feasible scheme to achieve the self-takeoff of large-scale flapping-wing robots without sacrificing flight performance and payload. Nature often presents astonishing phenomena that break conventional cognition: after floating out of the water, ospreys can transition the mode from takeoff to high maneuverability flight only by wing flapping, without the leg force. Inspired by the takeoff process of ospreys, we proposed a bionic take-off strategy and achieved self-takeoff on a meticulously designed large-scale flapping-wing system for the first time. The rest of this paper is organized as follows:

In Section II, we propose and analyze a bio-inspired self-takeoff strategy for large-scale flapping-wing vehicles, which maximizes the characteristics of periodic aerodynamic forces by flapping. Section III introduces the flapping-wing system design and development, including the flapping-wing aircraft based on the take-off strategy of ospreys and the auxiliary platform with an adjustable initial angle that can actively separate the object to be tested. The following Section IV presents the results of the flight experiments and compares the take-off characteristics of different thrust-to-weight ratios and initial pitch angles.

II. Ospreys-inspired take-off strategy and theoretical analysis

In this section, we first describe the biological characteristics of ospreys and the self-takeoff strategy of its takeoff from water. Then we propose a theoretical model with periodic variation characteristics of aerodynamic force, which is used to explain the requirements in the takeoff process. Finally, we discussed the effects of thrust-to-weight ratio and initial pitch angle on take-off based on the theoretical model.

This work is supported by the National Natural Science Foundation of China(Grant No. 62233001), Program of Shenzhen Peacock Innovation Team (Grant No. KQTD20210811090146075) and Shenzhen excellent scientific and technological innovation talent training project (Grant No. RCJC20200714114436040)

The authors are with the School of Mechanical Engineering and Automation, Harbin Institute of Technology, Shenzhen 518055, China. They are also with Guangdong Provincial Key Laboratory of Intelligent Morphing Mechanisms and Adaptive Robots, and Guangdong Key Laboratory of Intelligent Morphing Mechanisms and Adaptive Robotics. (perzhen@hit.edu.cn)

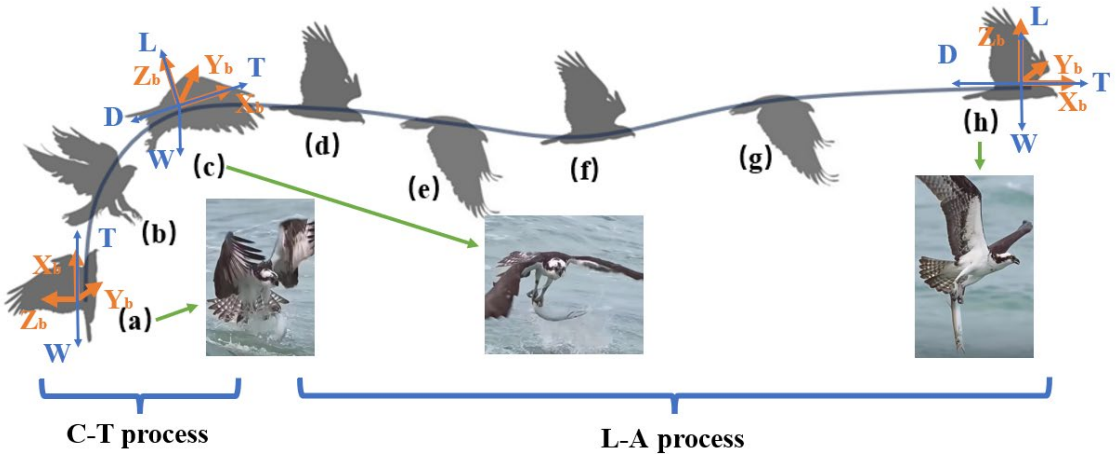

Fig. 1. As shown by the trajectory in the sagittal (x–z) plane during a representative take-off flight, ospreys start climbing with an initial pitch angle close to 90 degrees, then turn to level attitude through several powerful wing beats (C-T process). During the level acceleration process (L-A process), the height of the osprey may drop slightly, but this will not cause it to fall back into the water. As the flight speed increases, the lift gradually balances with gravity.

A. Ospreys -inspired takeoff strategy

The osprey, is a large raptor, reaching more than 60 cm (24 in) in length and 180 cm (71 in) across the wings. The osprey's diet consists almost exclusively of fish. It possesses specialized physical characteristics and unique behavior in hunting its prey. This characteristic makes its takeoff process from the water after predation have distinct features, which has important reference significance for the research of self-takeoff of flapping-wing robots [11], [12].

Unlike most birds that take off by bouncing off their legs, ospreys have no ground support when they take off from the water, and the take-off process is accomplished by flapping their wings. By observing and analyzing the take-off process of ospreys, we found that the takeoff process is fast and exquisite: it only takes 8 flaps, lasting about 2.5s, to go from leaving the water surface to steady flight, as shown in Fig. 1.

Before taking off, the osprey first emerges from the water with a large pitch angle, then performs several pre-flaps, which are generally small in amplitude, mainly to shake off the water on the feathers and adjust the body posture. Then the osprey increases the flapping amplitude and frequency, and for the sake of research, we call the flap that causes the body to leave the water surface as the first flap. During the first three flaps, the osprey slowly and slightly rose in height while the horizontal displacement remained almost unchanged. Meanwhile, the pitch angle tilted to 0°. We named this process as climbing-tilting process (C-T process). Then, the osprey uses 5 flaps to accelerate in the horizontal direction. Since the airspeed is almost zero when the acceleration starts, the osprey's flight height first drops slightly, then slowly increases as the flight speed increases. The flapping amplitude and frequency gradually decrease until the flight speed no longer increases. This process is called the level acceleration process (L-A process).

This take-off strategy of the Osprey allows it to take advantage of the aerodynamic efficiency improvement brought by speed during take-off. Compared with direct vertical climb, it saves more flight energy and reduces the biological requirements for muscle load capacity.

This take-off strategy is mainly influenced by the following three factors [13]- [15]:

- The flapping-wing robot needs enough thrust to meet the climbing requirement of the C-T stage.
- The initial pitch angle affects the starting condition and the direction of the aerodynamic resultant force of the whole process, thus changing the take-off process.
- The flapping wing aircraft needs to have good pitch maneuverability so that it can tilt the pitch angle to 0 in the C-T process, and maintain the attitude in the L-A process.

Next, we will conduct a theoretical analysis of the take-off process through dynamic modeling, and discuss the effects of thrust-to-weight ratio and initial pitch angle. The design of the pitch maneuverability will be elaborated in section III.

B. DynamicModeling

To clarify the role of flapping alternating aerodynamic force in the take-off process, we establish the flapping dynamics equation in the ground coordinate system as shown in Fig. 2, and introduce a time-varying force function, as follows:

$$m\ddot{z}(t) = T(t)\sin\theta(t) + L(t)\cos\theta(t) - mg - D \tag{1}$$

where z is the height of the center-of-mass.

For the take-off process, since the airspeed is almost zero, the drag $D = 0$, the thrust T and lift L can be expressed by Fourier series, as follows:

$$\begin{aligned} T(t) &= T_0 + T_{11}\sin(\omega_T t) + T_{12}\cos(\omega_T t) + T_{21}\sin(2\omega_T t) + T_{22}\cos(2\omega_T t)... \\ L(t) &= L_0 + L_{11}\sin(\omega_L t) + L_{12}\cos(\omega_L t) + L_{21}\sin(2\omega_L t) + L_{22}\cos(2\omega_L t)... \end{aligned} \tag{2}$$

Where $\omega_T = 2\omega_L = 2\omega$, ω is the angular velocity with one wing flapping cycle as the period. By the property of the Fourier series, T_0 means the time-averaged thrust, L_0 means the time-averaged lift. As the aerodynamic force of flapping is symmetrical, the time-averaged lift $L_0 \approx 0$. In this case, the lift and drag can be simplified as follows:

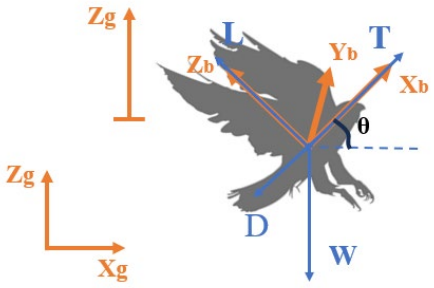

Fig. 2. The subscript g represents the ground coordinate system, subscript b represents the body coordinate system. Because the airspeed is almost zero at take-off, the direction of lift coincides with the Z_b axis at this time, and the direction of thrust is along the X_b axis.

$$\begin{cases} T(t) = \overline{T} + T_{amp}\sin(\omega_T t) \\ L(t) = L_{amp}\sin(\omega_L t) \end{cases} \tag{3}$$

T_{amp}、L_{amp} are the amplitude thrust and amplitude lift, respectively. Amplitude thrust and lift mean half of the difference between the maximum and minimum values in a cycle. $\overline{T}$ is the time-averaged thrust.

To analyze the effect of aerodynamic force, we assume that the pitch angle θ remains constant within the climbing process, that is, $\theta(t) = \theta_0$. By substituting the above conditions into the equation (1), and dividing both sides of the equation by $W = mg$, we obtain the vertical dynamics equation of each flapping cycle:

$$\begin{aligned} \frac{\ddot{z}(t)}{g} &= \frac{(\overline{T} + T_{amp}\sin(\omega_T t))\sin\theta_0 + L_{amp}\sin(\omega_L t)\cos\theta_0}{mg} - 1 \\ &= (\frac{\overline{T}}{W}\sin\theta_0 - 1) + \frac{T_{amp}}{W}\sin(\omega_T t)\sin\theta_0 + \frac{L_{amp}}{W}\sin(\omega_L t)\cos\theta_0 \end{aligned} \tag{4}$$

Where $\frac{\overline{T}}{W}, \frac{T_{amp}}{W}, \frac{L_{amp}}{W}$ are the time-averaged thrust-to-weight ratio, amplitude thrust-to-weight ratio, and amplitude lift-to-weight ratio, respectively. The vertical velocity and displacement can be obtained by integrating with the initial conditions of $\dot{z}(0) = 0$, $z(0) = 0$, as follows:

$$\begin{cases} \frac{\dot{z}(t)}{g} = (\frac{\overline{T}}{W}\sin\theta_0 - 1)t + \left(\frac{T_{amp}}{W\omega_T}\sin\theta_0 + \frac{L_{amp}}{W\omega_L}\cos\theta_0\right) \\ \quad -\left(\frac{T_{amp}}{W\omega_T}\cos(\omega_T t)\sin\theta_0 + \frac{L_{amp}}{W\omega_L}\cos(\omega_L t)\cos\theta_0\right) \\ \frac{z(t)}{g} = (\frac{\overline{T}}{W}\sin\theta_0 - 1)\frac{t^2}{2} + \left(\frac{T_{amp}}{W\omega_T}\sin\theta_0 + \frac{L_{amp}}{W\omega_L}\cos\theta_0\right)t \\ \quad -\left(\frac{T_{amp}}{W{\omega_T}^2}\sin(\omega_T t)\sin\theta_0 + \frac{L_{amp}}{W{\omega_L}^2}\sin(\omega_L t)\cos\theta_0\right) \end{cases} \tag{5}$$

C. Thrust-to-weight ratio demanded for self-takeoff

The C-T process provides the initial altitude for the aircraft, which serves as the basis for the subsequent flight. In comparison, the gravity that needs to be overcome during climbing is much larger than the aerodynamic drag, thus the primary condition for self-takeoff is that the drone must increase its altitude from a stationary state.

Taking the first flap as an example, $\theta_i = \theta_0 = \frac{\pi}{2}$, then the equation (5) can be simplified as follows:

$$\begin{cases} \frac{\ddot{z}_i(t)}{g} = (\frac{\overline{T}}{W} - 1) + \frac{T_{amp}}{W}\sin(\omega_T t) \\ \frac{\dot{z}_i(t)}{g} = (\frac{\overline{T}}{W} - 1)t + \frac{T_{amp}}{W\omega_T} - \frac{T_{amp}}{W\omega_T}\cos(\omega_T t) \\ \frac{z_i(t)}{g} = (\frac{\overline{T}}{W} - 1)\frac{t^2}{2} + \frac{T_{amp}}{W\omega_T}t - \frac{T_{amp}}{W{\omega_T}^2}\sin(\omega_T t) \end{cases} \tag{6}$$

It is intriguing that when the time-averaged thrust-to-weight ratio $\frac{\overline{T}}{W} \le 1$, $\ddot{z}(t), \dot{z}(t)$ fluctuate between positive and negative values along the flapping process, but there is a situation where $z(\frac{2\pi}{\omega}) - z(0) > 0$ when $\frac{\overline{T}}{W} > 1 - \frac{T_{amp}}{2\pi W}$. n represents the number of flaps during the C-T process. This indicates that even if the time-averaged thrust-to-weight ratio is less than 1, the flapping-wing aircraft can still go up, because of the burst effect of wing flapping, as shown in Fig. 3. Due to the take-off strategy, the flapping-wing aircraft can quickly complete the attitude tilt, so as long as it raises a sufficient altitude in the first flapping cycle, the aircraft can be maintained to complete the take-off process. Therefore, $\frac{\overline{T}}{W} > 1 - \frac{T_{amp}}{2\pi W}$ is a necessary condition of self-takeoff.

D. Effects of initial pitch angle

The above analysis is carried out under the assumption of $\theta_0 = \frac{\pi}{2}$, which is a special case of vertical take-off. More generally, different initial pitch angles will also affect the self-takeoff process. As can be seen from the above analysis, the displacement expression of the general case can be simplified as:

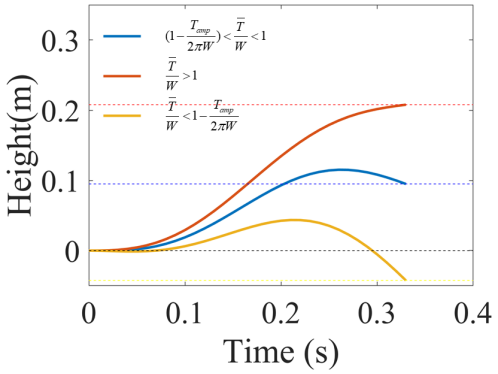

Fig. 3 The height change of the flapping wing in a flapping cycle under different time-average thrust-to-weight ratio conditions.

$$\frac{z(t)}{g}=(\frac{\overline{T}}{W}\sin\theta_0-1)\frac{t^2}{2}+\left(\frac{T_{amp}}{W\omega_T}\sin\theta_0+\frac{L_{amp}}{W\omega_L}\cos\theta_0\right)t \quad (7)$$

By substituting the takeoff requirement $z(\frac{2\pi}{\omega})-z(0)>0$ into equation(7), the inequality of the time-averaged thrust-to-weight ratio under different initial pitch angle conditions can be obtained:

$$\frac{\overline{T}}{W}>\frac{1-\frac{L_{amp}}{\pi W}\cos\theta_0}{\sin\theta_0}-\frac{T_{amp}}{2\pi W} \quad (8)$$

Compared with the thrust-to-weight ratio requirement $\frac{\overline{T}}{W}>1-\frac{T_{amp}}{2\pi nW}$, if $\frac{1-\frac{L_{amp}}{\pi W}\cos\theta_0}{\sin\theta_0}<1$, it seems that reducing the pitch angle appropriately is beneficial to self-takeoff. But considering the final speed $\dot{z}(\frac{2\pi}{\omega})=(\frac{\overline{T}}{W}\sin\theta_0-1)\bullet 2\pi$, reducing the initial pitch angle will cause the drone to have a strong downward trend, which is very unfavorable to the level flight acceleration process, and the flight test also confirmed this phenomenon.

III. System Design and Development

This section introduces the design and development of the flapping wing system, including the auxiliary platform of self-takeoff and the experiment prototype.

A. Auxiliary platform of self-takeoff development

To explore the impact of the initial pitch angle on the self-takeoff process, we designed an auxiliary platform that can adjust the release angle of the drone.

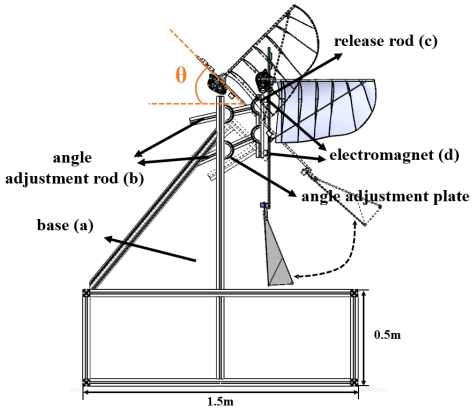

Fig. 4. The auxiliary platform consists of three parts: base (a), angle adjustment rod (b), and release rod (c).

Before takeoff, the flapping-wing aircraft needs to flap at high power in a stable initial pitch angle state, which generates a maximum aerodynamic load of more than 30N (as shown in Fig. 7(b)), posing a great challenge to the design of the release mechanism. Moreover, if the release process affects the drone's attitude, it will cause the attitude to overturn, leading to a crash. At the same time, the release device should not add too much extra structure to the prototype. Therefore, a stable auxiliary platform and a clever release device are the keys to self-takeoff.

We use an aluminum alloy width of 30mm to build a structure, forming a rectangular base with a size of 1.5m*1m*0.5m at the bottom, which can greatly reduce the vibration problem caused by the flapping of the test prototype. In order to explore the self-takeoff characteristics under different initial pitch angles, we achieve the pitch angle adjustment capability of 0°-120° with four angle adjustment plates.

Based on the above requirements, we consider an electromagnetic separation scheme that has good control ability and does not add extra mechanical structure. The magnetism of the electromagnet can be controlled by turning on and off the electric current, which also solves the problem of controlling the release timing. We use two electromagnets with a maximum attraction of 30kg, and set up them on the release rod at a distance of 50cm, using 3D-printed parts. Two low-carbon steel plates with a thickness of 2mm are set up on the flapping-wing robot and stick to the electromagnets.

B. Flapping-wing prototype design

How to achieve the thrust-to-weight ratio required for self-takeoff and pitch maneuvering during takeoff brings new challenges to the prototype design. The prototype design is based on HIT-Hawk, which is an eagle-scale flapping-wing aerial vehicle developed by Harbin Institute of Technology (Shenzhen), as shown in Fig. 5(a). The main purpose of HIT-Hawk is to research the design theory and experimental methods of large-scale flapping-wing robots.

The take-off weight of HIT-Hawk is 1.15 kg and the time-averaged thrust is less than 5N. Such a thrust-to-weight ratio is beneficial for improving endurance, but far from enough for self-takeoff. Similarly, to reduce the drag caused by the tail, HIT-Hawk minimizes the tail area and arm length in the design, making it difficult to perform continuous pitch maneuvers, which do not meet the self-takeoff requirements. Therefore, based on HIT-Hawk, we designed the prototype according to the requirements of self-takeoff for aircraft performance.

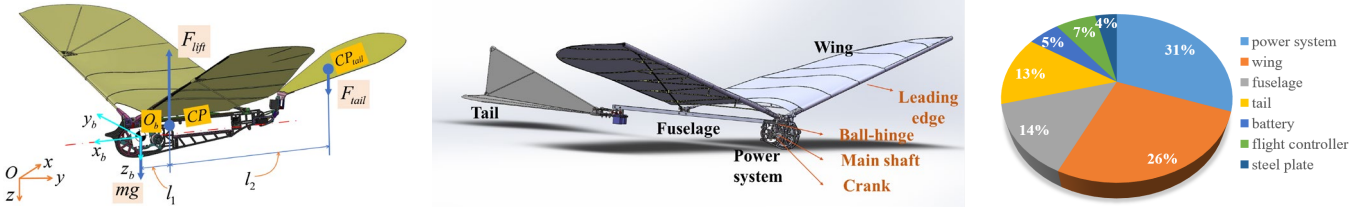

(a) (b) (c)

Fig. 5 (a) 3D mechanical design of HIT-Hawk. (b) 3D mechanical design of the self-takeoff prototype. (c) Weight distribution of each part of the prototype.

The first improvement is on the power system. According to the flapping wing theory, increasing the flapping frequency and amplitude can effectively increase the thrust [16], [17], but this requires the power system to have a greater load capacity. As shown in Fig. 5(b), in the design of the power system, we use a three-stage reducer with a reduction ratio of 56 and use lightweight titanium alloy to make the main shaft, which can withstand a flapping frequency of 3Hz and input power of 500W. The wing's leading edge is connected by a ball-hinge with a crank, forming a four-bar linkage. Changing the length of the crank and the ball-hinge can increase the flapping amplitude to 59°. To reduce the load of the wing inertia on the power components, we designed a wing with a wingspan of 1.8m, using a 7mm diameter leading edge rod and 2mm thick carbon fiber ribs to increase the strength.

Next, we try to obtain greater pitch maneuverability by increasing the tail volume. The tail volume calculation formula is as follows:

$$V_H = \frac{l_H S_H}{c_A S} \tag{10}$$

Where l_H, S_H, c_A, S are the tail arm, area of tail, wing chord, and area of wing, respectively.

By using a larger tail and a longer fuselage, the full-moving tail's area reaches 10.8dm^2, the tail arm is 942mm, which makes the tail volume reach 0511. Such a tail volume is similar to the fixed-wing aircraft with high maneuverability, which can generate enough pitch moments at low airspeed.

Finally, we design the fuselage and minimize unnecessary structural weight as much as possible. The fuselage is composed of 10mm square hollow carbon fiber rods, which have higher specific stiffness and strength so that less weight cost is required to ensure structural safety.

The weight distribution of each part of the prototype is shown in Fig. 5(c). The parameters of HIT-Hawk and the self-takeoff prototype are compared as shown in TABLE I.

In this study, we use a self-developed flight controller HIT-Decider-V1 with a Six-Axis (Gyro & Accelerometer) MEMS MotionTracking Devices MPU6050 on the flight platform. (Fig. 6)This sensor has a 500Hz digital-output of 6-axis MotionFusion data, which is used to obtain the motions of the drone. High-precision NEO3PRO GPS is used to measure the position of the drone. Power component collects voltage and current, to evaluate the power consumption.

TABLE I. PARAMETERS OF HIT-HAWK AND THE PROTOTYPE

Parameters	*HIT-Hawk*	*Prototype*
Length (cm)	75	125
Wingspan (cm)	200	180
Mean chord length (cm)	31.6	33.2
Weight (g)	1150	870
flapping frequency(Hz)	2	3
flapping amplitude(deg)	30.81	59
Cruising power(W)	43	54
Tail volume	0.114	0.511
Thrust-to-weight ratio(avg)	0.444	0.876

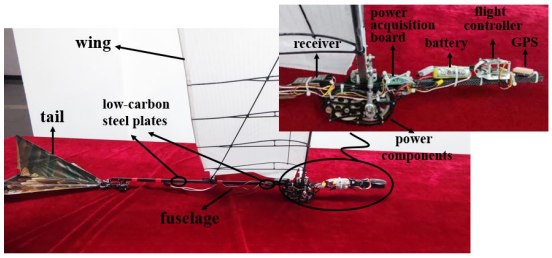

Fig. 6 Prototype configuration and payload position

C. thrust measurement

According to the theoretical analysis in Section II, the thrust-to-weight ratio satisfying $\frac{\overline{T}}{W} > 1 - \frac{T_{amp}}{2\pi W}$ is a necessary condition for self-takeoff. Therefore, to ensure the aerodynamic force of the prototype, we used a six-dimensional force test platform to measure the aerodynamic force of the wing under different flapping amplitudes (40°-59°) and flapping frequencies (1.5Hz-3.5Hz). The results show that the time-averaged thrust increases linearly with the increase of flapping amplitude and frequency. The instantaneous thrust shows alternating high and low peaks within a flapping cycle, which is due to the bending of the airfoil. Under the design conditions of the prototype, the time-average thrust is 7.196N, and the amplitude thrust is 8.766N, as shown in Fig. 7(b). Substituting the experimental results into the thrust-to-weight ratio inequality, the average thrust-to-weight ratio requirement is $\frac{\overline{T}}{W} > 0.836$. The prototype thrust-to-weight ratio in this paper is 0.876, which shows that the prototype design meets the self-takeoff requirements.

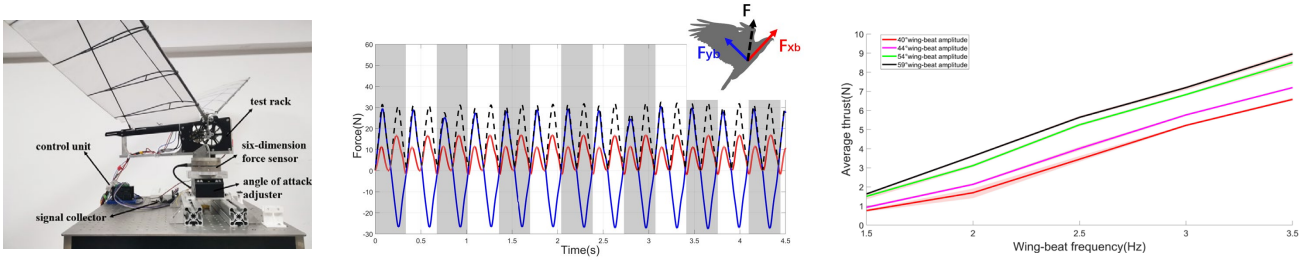

(a) (b) (c)

Fig. 7. (a)The core of the platform is a six-dimensional force/torque sensor, using the M3816BH SN6472 model from SRI. The electrical signal is converted into a digital signal by a signal acquisition device, and stored in the computer after being integrated by the control unit. (b) 3Hz flapping frequency, 59° flapping amplitude test results without stream flow. (c)Time-averaged thrust under flapping frequency range 1.5-3.5Hz and wing-beat frequency range 40°-59°.

IV. FLIGHT EXPERIMENTS

To validate the proposed method, firstly, we experiment the take-off performance of 90° initial pitch angle under different take-off weights of 870g, 920g, and 970g, which means the time-averaged thrust-to-weight ratio of 0.844, 0.798, 0.757. Afterward, the experiment that the drone takeoff at different initial pitch angles of 90°, 75°, 60°, and 45° under the weight of 870g was performed. Different test weights were adjusted by fixing weights at the center of gravity position, while the initial pitch angle was adjusted by the test stand.

The experiments were performed outdoors because the L-A process requires a long acceleration distance. The coordinates were 22°35'15.7"N 113°58'01.7"E, on a sunny day, with a 32°C maximum temperature and hardly a breath of air.

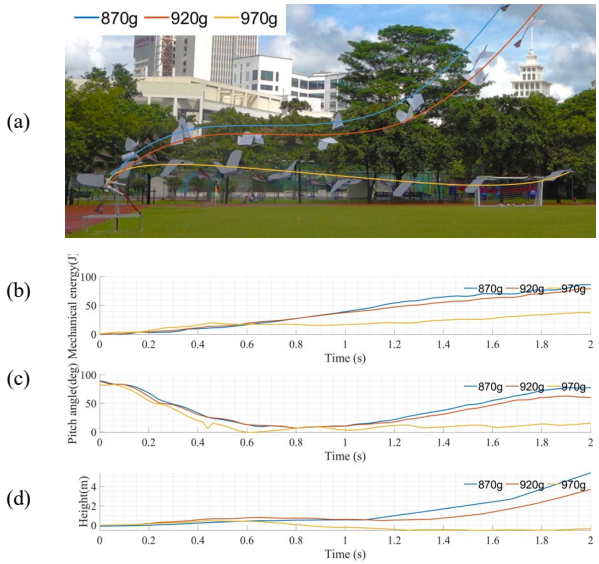

Fig. 8 Flight experiment results under different thrust-to-weight ratios. (a) Flight experiments under different thrust-to-weight ratios, each prototype photo time interval is 0.5s. (b) The curve of mechanical energy versus time. (c) The curve of pitch angle versus time. (d) The curve of height versus time.

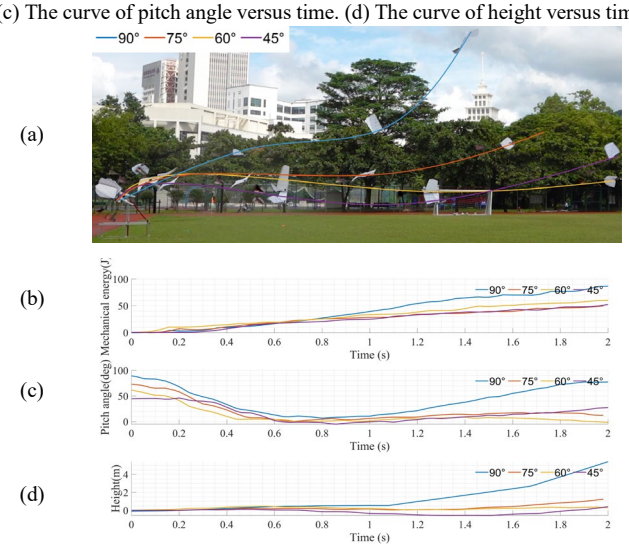

Fig. 9 Flight result experiment under different initial pitch angles. (a) Flight experiments under different thrust-to-weight ratios, each prototype photo time interval is 0.5s. (b) The curve of mechanical energy versus time. (c) The curve of pitch angle versus time. (d) The curve of height versus time.

A. Flight experiment under different thrust-to-weight ratios

We analyzed the flight data within 2s after self-takeoff. The flight experiments under different thrust-to-weight ratios show that as the thrust-to-weight ratio decreases, the height increase of the prototype in the C-T stage becomes smaller and smaller. When the thrust-to-weight ratio drops to 0.757, the height of the prototype in the L-A stage is sometimes lower than the takeoff height. This indicates that at this time, the prototype must release extra gravitational potential energy to complete self-takeoff. In the flight experiment with a thrust-to-weight ratio of 0.798, the prototype also completed self-takeoff. This is 4.76% different from the requirement of the thrust-to-weight ratio calculated by the theoretical model. We supposed that this error may come from process errors, environmental interference, etc. The mechanical energy data is used to analyze the energy utilization rate. At the same flight time, the higher the mechanical energy, the more useful energy the prototype obtains. As the thrust-to-weight ratio decreases, the energy utilization rate of the self-takeoff process becomes lower, which indicates that increasing thrust and reducing weight are beneficial to reducing the energy consumption of the self-takeoff process.

B. Flight experiment under different initial pitch angle

We used the same method to analyze the experimental data under different initial pitch angles. The results show that as the initial pitch angle decreases, the self-takeoff process becomes gradually difficult. When the initial pitch angle drops to 60°, the A-L process shows a flight height lower than the takeoff height, indicating that at this time, the prototype can no longer complete self-takeoff without consuming extra potential energy. We also found that as the initial pitch angle decreases, the energy utilization efficiency also gradually decreases. This is due to the fact that as the initial pitch angle decreases, the C-T process time becomes shorter, resulting in the prototype not being able to quickly enter a stable flight state at the A-T process.

V. CONCLUSION

Inspired by flying animals, flapping-wing aircraft have their unique advantages in self-powered takeoff, namely, they can complete the takeoff with a time-averaged thrust-to-weight ratio of less than 1. The application of this biological characteristic can obtain many benefits, such as taking off with more payload under lower energy consumption and reducing the air resistance caused by extra parts such as bird legs, which has a broad prospect for the design of aircraft with limited weight and power. In this work, we are the first to achieve a self-takeoff of the eagle-scale flapping-wing aircraft. We have demonstrated that this eagle-like flapping-wing aircraft can take off with a low time-averaged thrust-to-weight ratio by appropriate aerodynamic configuration and flight strategy. The basic dynamic principles and design schemes can be extended to any flapping-wing aircraft with similar configurations. In future work, besides self-takeoff, we will try more aggressive maneuvers to expand the application of flapping-wing aircraft in more complex environments and conditions.

REFERENCES

[1] Zufferey, R., Tormo-Barbero, J., Feliu-Talegón, D. et al. How ornithopters can perch autonomously on a branch. Nat Commun 13, 7713 (2022).

[2] Erzhen Pan, Hui Xu, Han Yuan, Jianqing Peng, Wenfu Xu, HIT-Hawk and HIT-Phoenix: Two kinds of flapping-wing flying robotic birds with wingspans beyond 2 meters. Biomimetic Intelligence and Robotics, Volume 1,2021, 100002, ISSN 2667-3797.

[3] Wenfu XU, Erzhen PAN, Juntao LIU, Yihong LI, Han YUAN, Flight control of a large-scale flapping-wing flying robotic bird: System development and flight experiment. Chinese Journal of Aeronautics, Volume 35, Issue 2, 2022, Pages 235-249, ISSN 1000-9361.

[4] A. Chen, B. Song, Z. Wang, D. Xue, and K. Liu, "A Novel Actuation Strategy for an Agile Bioinspired FWAV Performing a Morphing-Coupled Wingbeat Pattern," in IEEE Transactions on Robotics, vol. 39, no. 1, pp. 452-469, Feb. 2023.

[5] B. Cheng and X. Deng, "Translational and Rotational Damping of Flapping Flight and Its Dynamics and Stability at Hovering," in IEEE Transactions on Robotics, vol. 27, no. 5, pp. 849-864.

[6] Yao-Wei Chin, et al. “Efficient flapping wing drone arrests high-speed flight using post-stall soaring”, Science Robotics, vol. 5, no. 41, eaba2386, 2020.

[7] H. V. Phan, Q. V. Nguyen, H. C. Park, N. S. Goo, and D. Byun, "Improvement of stability for vertical take-off of an insect-mimicking flapping-wing system," 2011 8th International Conference on Ubiquitous Robots and Ambient Intelligence (URAI), Incheon, Korea (South), 2011, pp. 872-872.

[8] Chin, D.D., Lentink, D., Birds repurpose the role of drag and lift to take off and land. Nat Commun 10, 5354 (2019).

[9] Angela M. Berg, Andrew A. Biewener; Wing and body kinematics of takeoff and landing flight in the pigeon (Columba livia). J Exp Biol 15 May 2010; 213 (10): 1651–1658.

[10] F.H. Heppner and JG. Anderson, "Leg thrust important in flight take-off in the pigeon", J Exp Biol, vol. 114, pp. 285-288, 1985.

[11] Robbins, C. S.; Bruun, Bertel; Zim, H. S.; Singer, A. (1983). Birds of North America (Revised ed.). New York: Golden Press. pp. 78–79. ISBN 0-307-37002-X

[12] T. E. Dennis. (2007) Reproductive activity in the Osprey (Pandion haliaetus) on Kangaroo Island, South Australia. Emu - Austral Ornithology 107:4, pages 300-307.

[13] T. Sato, T. Nakano, and N. Takesue, "Study on Self-Takeoff of a Flapping Robot without Running: Influence of the Initial Pitch Angle on the Takeoff Trajectory," 2019 IEEE International Conference on Robotics and Biomimetics (ROBIO), Dali, China, 2019, pp. 65-70.

[14] O. A. Hudson et al., "Bio-inspired jumping maneuver for launching flapping wing micro air vehicles," 2018 IEEE International Conference on Autonomous Robot Systems and Competitions (ICARSC), Torres Vedras, Portugal, 2018, pp. 104-109.

[15] Hudson, O.A.; Fanni, M.; Ahmed, S.M.; Sameh, A. Autonomous Flight Take-off in Flapping Wing Aerial Vehicles. J. Intell. Robot. Syst. 2020, 98, pp.135–152.

[16] F. Platzer, Flapping Wing Aerodynamics: Progress and Challenges. AIAA Journal 2008 46:9, 2136-2149

[17] Longfei Zhao and Zongxia Jiao, Efficiency-Optimal Rigidity Configuration of Passive Torsional Flapping Wings. AIAA Journal 2021 59:11, 4354-4366